genesis 54:350–358 (2016)

TECHNOLOGY REPORT

Pdgfrb-Cre Targets Lymphatic Endothelial Cells of Both Venous and Non-venous Origins

Maria H. Ulvmar, Ines Martinez-Corral, Lukas Stanczuk, and Taija Mäkinen*

Department of Immunology Genetics and Pathology, Uppsala University,
Dag Hammarskjöldsväg 20, 751 85, Uppsala, Sweden

Received 12 February 2016; Revised 16 March 2016; Accepted 2 April 2016

Abstract: The *Pdgfrb-Cre* line has been used as a tool to specifically target pericytes and vascular smooth muscle cells. Recent studies showed additional targeting of cardiac and mesenteric lymphatic endothelial cells (LECs) by the *Pdgfrb-Cre* transgene. In the heart, this was suggested to provide evidence for a previously unknown nonvenous source of LECs originating from yolk sac (YS) hemogenic endothelium (HemEC). Here we show that *Pdgfrb-Cre* does not, however, target YS HemEC or YS-derived erythro-myeloid progenitors (EMPs). Instead, a high proportion of ECs in embryonic blood vessels of multiple organs, as well as venous-derived LECs were targeted. Assessment of temporal Cre activity using the *R26-mTmG* double reporter suggested recent occurrence of *Pdgfrb-Cre* recombination in both blood and lymphatic ECs. It thus cannot be excluded that *Pdgfrb-Cre* mediated targeting of LECs is due to de novo expression of the *Pdgfrb-Cre* transgene or their previously established venous endothelial origin. Importantly, *Pdgfrb-Cre* targeting of LECs does not provide evidence for YS HemEC origin of the lymphatic vasculature. Our results highlight the need for careful interpretation of lineage tracing using constitutive Cre lines that cannot discriminate active from historical expression. The early vascular targeting by the *Pdgfrb-Cre* also warrants consideration for its use in studies of mural cells. genesis 54:350–358, 2016. © 2016 The Authors. Genesis Published by Wiley Periodicals, Inc.

Key words: lymphangiogenesis; lymphvasculogenesis; vascular development; mural cell

INTRODUCTION

The *Pdgfrb-Cre* line (Foo *et al*., 2006), where Cre recombinase expression is driven by a transgenic fragment of the gene for platelet-derived growth factor receptor β (*Pdgfrb*), has been used extensively to specifically target mural cells, namely vascular smooth muscle cells, pericytes and hepatic stellate cells; examples are given in ref (Abraham *et al*., 2008; Foo *et al*., 2006; Greif *et al*., 2012; Henderson *et al*., 2013; Jeansson *et al*., 2011; Kogata *et al*., 2009; Siegenthaler *et al*., 2013; Stenzel *et al*., 2009; Ye *et al*., 2009; You *et al*., 2014). We (Stanczuk *et al*., 2015) and others (Klotz *et al*., 2015) recently showed that *Pdgfrb-Cre* unexpectedly also targets a large proportion of embryonic lymphatic endothelial cells (LECs) in the developing mesentery (Stanczuk *et al*., 2015) and the heart (Klotz *et al*., 2015). These observations were made in the context of the startling discovery that LECs in the heart (Klotz *et al*., 2015), mesentery (Stanczuk *et al*. 2015), and skin (Martinez-Corral *et al*., 2015), not only develop through lymphangiogenic sprouting from a venous blood vascular source, which has previously been the only known mechanism for lymphatic vessel formation in mammals (Srinivasan *et al*., 2007), but also through the assembly of nonvenous derived LEC progenitors.

Current address for Lukas Stanczuk: Astex Pharmaceuticals, 436 Cambridge Science Park, Milton Road, Cambridge CB40QA, United Kingdom.

*Correspondence to: Taija Mäkinen, Department of Immunology Genetics and Pathology, Uppsala University, Dag Hammarskjöldsväg 20, 752 85, Uppsala, Sweden., E-mail: taija.makinen@igp.uu.se

Contract grant sponsor: European Research Council, Contract grant number: ERC-2014-CoG-646849; Contract grant sponsor: Swedish Research Council

Published online 6 April 2016 in
Wiley Online Library (wileyonlinelibrary.com).
DOI: 10.1002/dvg.22939

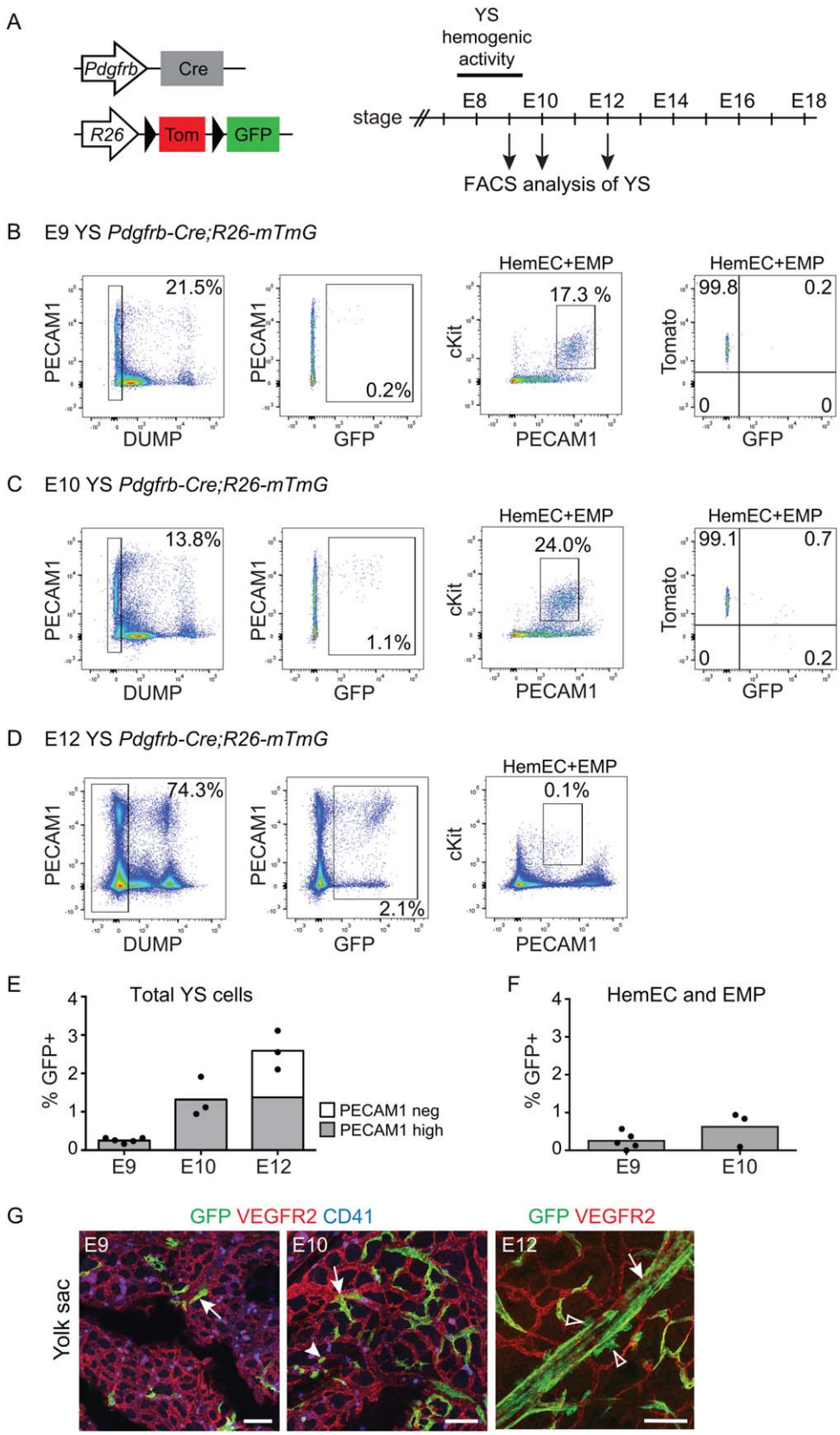
A
Pdgfrb
Cre
R26
Tom
GFP
YS hemogenic activity
stage
E8
E10
E12
E14
E16
E18
FACS analysis of YS
B E9 YS Pdgfrb-Cre;R26-mTmG
21.5%
PECAM1
DUMP
0.2%
GFP
HemEC+EMP
17.3 %
cKit
PECAM1
HemEC+EMP
99.8
0.2
0
0
Tomato
GFP
C E10 YS Pdgfrb-Cre;R26-mTmG
13.8%
1.1%
24.0%
HemEC+EMP
99.1
0.7
0
0.2
D E12 YS Pdgfrb-Cre;R26-mTmG
74.3%
2.1%
0.1%
HemEC+EMP
E
Total YS cells
% GFP+
PECAM1 neg
PECAM1 high
E9
E10
E12
F
HemEC and EMP
G
GFP VEGFR2 CD41
GFP VEGFR2
Yolk sac
E9
E10
E12

FIG. 1.

In the mesentery, our lab traced the non-venous LEC origin to a hemogenic endothelial cell (HemEC) source. This conclusion was based on positive lineage tracing using the endothelial specific *Pdgfb-CreER^{T2}* line induced at embryonic day (E)8-E9, together with positive tracing of E10-E11 induced *cKit-CreER^{T2}* (Stanczuk *et al*., 2015). cKit is a marker associated with HemECs and HemEC-derived hematopoietic progenitors from all known hemogenic sites of the embryo and the yolk sac (YS) (Antas *et al*., 2013; Medvinsky et al., 2011). In the heart, *Pdgfrb-Cre* induced labeling, together with positive labeling with *Vav-Cre*, a pan-hematopoietic lineage marker, and E7 induced *Csf1r1-MeriCreMer*, which traces YS-derived myeloid cells (Gomez Perdiguero et al., 2015; Hoeffel et al., 2015), was proposed to indicate YS HemEC as the source of cardiac LECs (Klotz et al., 2015).

Based on the highly efficient ability of *Pdgfrb-Cre* to target non-venous derived mesenteric LECs and lymphatic vessels (Stanczuk et al., 2015), along with the suggested YS HemEC origin of the *Pdgfrb-Cre* labeled LECs in the heart (Klotz et al., 2015), we set out to carefully evaluate the suggested ability of *Pdgfrb-Cre* to trace YS-derived HemEC-progenitors (Klotz et al., 2015) and its potential as a specific lineage marker for non-venous derived LEC progenitors. Here we demonstrate that *Pdgfrb-Cre* is not a valid tool for tracing YS HemEC-activity or YS derived progenitors, showing minimal expression in YS ECs before E12 and no tracing of the early YS-derived myeloid lineages. Furthermore, we show that *Pdgfrb-Cre* positive tracing cannot differentiate between non-venous and venous derived LEC progenitors, since it targets the cardinal vein, which is a known source of venous derived LECs. Unexpectedly, our data demonstrate that *Pdgfrb-Cre* is induced in embryonic blood vessels already at E9, and the proportion of Cre-recombined endothelial cells increases during development in both blood and lymphatic vessels. Interpretation of phenotypes caused by *Pdgfrb-Cre*-induced gene deletion must thus take into account also the partial targeting of both BECs and LECs from early embryonic development.

RESULTS AND DISCUSSION

To examine if *Pdgfrb-Cre* allows tracing of YS HemEC and YS-derived progenitors we crossed the *Pdgfrb-Cre* mice with the *R26-mTmG* fluorescent reporter line and analyzed YS of embryos during and after the period of hemogenic activity (Fig. 1A) (Gomez Perdiguero E et al., 2015; Hoeffel et al., 2015; Medvinsky et al., 2011). The *R26-mTmG* reporter allows detection of Cre activity by the recombination-induced expression of membrane-bound green fluorescent protein (GFP) and inactivation of the red fluorescent protein Tomato expression (Muzumdar et al., 2007). Because of perdurance of the Tomato protein within the recombined cells, co-expression of Tomato and GFP can additionally help discern recent recombination (i.e. active expression) from lineage tracing (i.e. historical expression).

E9, E10, and E12 embryos were harvested and the YSs were dissected away from the embryo proper and the vitelline artery. After gentle digestion, the YSs were analysed by flow cytometry. Ter119 positive cells (primitive erythrocytes) and dead cells were gated away in one single dump channel (Fig. 1b–d). Analysis of E9 and E10 YSs showed a minimal proportion of GFP$^+$ *Pdgfrb-Cre*-recombined cells [0.27% ± 0.06% (E9; Fig. 1b,e) and 1.38% ± 0.46% (E10; Fig. 1c,e)], increasing slightly at E12 (2.59% ± 0.51%; Fig. 1d,e). At E9 and E10, the GFP$^+$ population contained only PECAM1^{high} cells (100% ± 0%; Fig. 1e). At E12 both endothelial (PECAM1^{high}) (53.4% ± 1.8%) and nonendothelial (PECAM1^{neg}) (46.6% ± 1.8%) cells showed recombination, likely reflecting expression of *Pdgfrb-Cre* in both YS ECs and mural cells (Fig. 1d,e). Immunofluorescence analysis of the YS confirmed the presence of rare, scattered GFP$^+$ ECs in E9 and E10 vasculature (Fig. 1g), while E12 embryos displayed both GFP$^+$ ECs and mural cells around larger arteries (Fig. 1g). However, although *Pdgfrb-Cre* did target rare ECs in the YS, analysis of the YS cKit$^+$ cell population, which includes both HemECs and YS-derived erythroid/myeloid progenitors (EMPs), did not support specific targeting of HemECs. A very low proportion of GFP$^+$ cells was observed both at E9

FIG. 1. *Pdgfrb-Cre* does not target hemogenic endothelium in the YS. (**A**) Schematic of the *Pdgfrb-Cre* transgene, *R26-mTmG* reporter construct and analyzed embryonic stages. The time frame for YS hemogenic activity is indicated. (**B**) Gating scheme and representative data for E9 *Pdgfrb-Cre;R26-mTmG* YSs ($n = 5$). Dump channel includes dead cells and erythrocytes (Ter119$^+$) (all stages), and macrophages (CD11b$^+$ F4/80$^+$) (E12 only). Dot plots from the left; (1) Live, non-erythrocyte gate; (2) Total proportion of GFP$^+$ cells in *Pdgfrb-Cre;R26-mTmG* YSs; (3) Gating of cKit positive cells (HemECs and EMPs); and (4) Tomato and GFP expression within HemEC/EMP population. (**C**) Gating scheme and representative data for E10 *Pdgfrb-Cre;R26-mTmG* YSs ($n = 3$), as described above (B). (**D**) Gating scheme and representative data for E12 *Pdgfrb-Cre, R26-mTmG* YSs ($n = 3$), Dot plots as above (B and C). cKit+ population is adjusted for differences in PECAM1 expression between E9, E10 and E12 YS, to account for downregulation of vascular markers in late EMPs (Gomez Perdiguero *et al*., 2015). Expression of Tomato and GFP in cKit$^+$ HemECs and EMPs is not displayed due to too low cell numbers of these cells at this stage. (**E, F**) Summary of data from E9, E10, and E12 embryos, showing the proportion of GFP$^+$ cells (**E**) or HemEC/EMPs (**F**) in the YS. The average percent of GFP$^+$ cells within PECAM1^{high} and PECAM1^{negative} populations is shown. The horizontal lines represent mean of all cells [$n = 5$ (E9) or $n = 3$ (E10 and E12)]. (**G**) Whole-mount immunofluorescence of E9, E10 and E12 yolk sacs showing scattered GFP$^+$ (green) endothelial cells (arrows, VEGFR2$^+$; red), hematopoietic cells (arrowheads, CD41$^+$; blue). GFP$^+$ mural cells (open arrowheads) are present at E12 around larger arteries that show high proportion of GFP$^+$ cells at this stage. Scale bars: 100 μm.

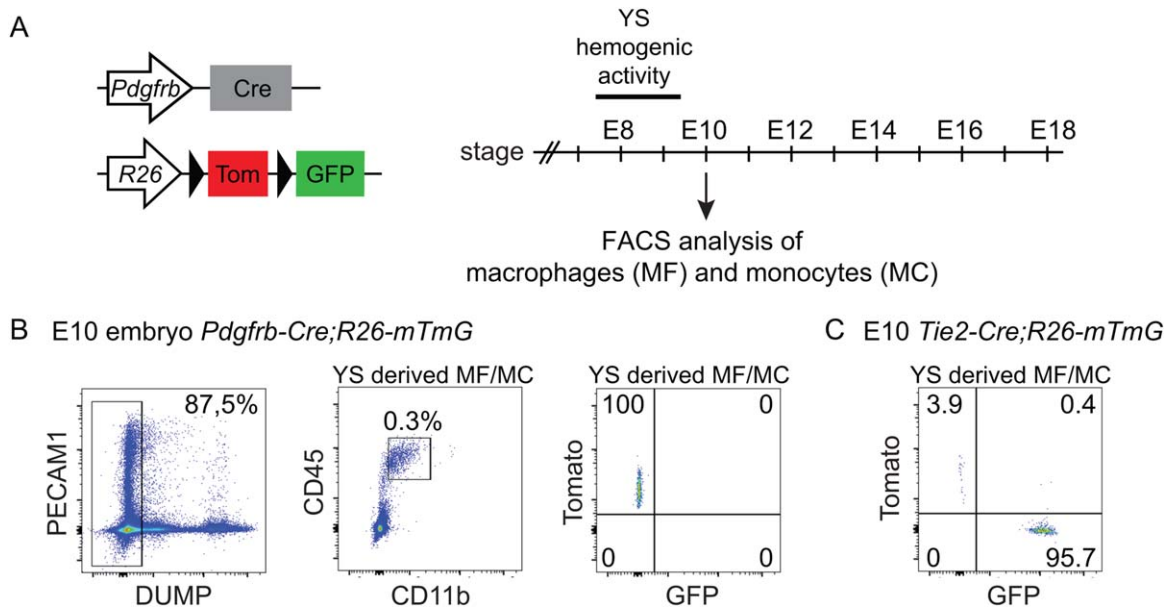

FIG. 2. *Pdgfrb-Cre* does not trace early YS-derived monocytes and macrophages. (**A**) Schematic of the *Pdgfrb-Cre* transgene, *R26-mTmG* reporter constructs and analyzed embryonic stages. The time frame for YS hemogenic activity is indicated. (**B**) Gating scheme and representative data for E10 *Pdgfrb-Cre;R26-mTmG* embryos ($n = 3$). Dump channel includes dead cells and erythrocytes (Ter119$^+$). Dot plots from the left: (1) Live, non-erythrocyte gate; (2) CD45^{high} CD11b$^+$ myeloid cells gated from total cells; (3) Expression of Tomato and GFP in E10 YS-derived monocytes (MC) and macrophages (MF). (**C**) Positive control for YS lineage tracing of E10 myeloid cells in *Tie2-Cre;R26-mTmG* embryo.

(0.25% ± 0.20%; Fig. 1b,f) and at E10 (0.63% ± 0.38%; Fig. 1c,f). Almost no cKit$^+$ cells were present in E12 YSs (Fig. 1d), consistent with the loss of hemogenic endothelial activity by this stage.

To follow up the analysis of *Pdgfrb-Cre* expression in the YS we also assessed if *Pdgfrb-Cre* can trace early macrophages and monocytes derived from the YS. For this purpose, we performed FACS analysis of *Pdgfrb-Cre;R26-mTmG* embryos at E10 (Fig. 2a), when the major pool of myeloid cells is YS-derived (Gomez Perdiguero et al., 2015; Hoeffel et al., 2015). In three out of three embryos we could not find any tracing of YS-derived monocytes and macrophages, defined by co-expression of the pan-myeloid marker CD11b and the pan-leukocyte marker CD45 (Fig. 2b). As a control, positive GFP tracing (96.1%) induced by *Tie2-Cre* is shown (Fig. 2c). The historical *Tie2-Cre* expression in the YS (E7-E9) is additionally demonstrated by loss of Tomato fluorescence in over 99% of the GFP$^+$ monocytes/macrophages (Fig. 2c). Taken together, these results exclude the possibility that *Pdgfrb-Cre* tracing of the lymphatic vasculature can be explained by a YS origin since the *Pdgfrb-Cre* transgene cannot efficiently label YS HemECs or EMPs in E9 and E10 YS, nor can it trace early E10 monocytes and macrophages that are known to derive from the YS (Gomez Perdiguero et al., 2015; Hoeffel et al., 2015).

Although *Pdgfrb-Cre* does not trace YS-derived HemECs, EMPs or YS-derived macrophage lineages, it would still be possible that it specifically targets non-venous derived LEC progenitors either through tracing of a non-venous derived LEC progenitor cell lineage within the embryo proper or through selective expression in non-venous derived LECs. To assess the specificity of *Pdgfrb-Cre* mediated targeting of LECs of different origins, we analysed Cre mediated recombination in the cardinal vein that provides a source of the first venous derived LECs, the peripheral longitudinal lymphatic vessel and the primordial thoracic duct, that are also referred to as the jugular lymph sacs (JLS) (Hagerling et al., 2013; Srinivasan et al., 2007; Yang et al., 2012). Immunofluorescence analysis of E13.5 *Pdgfrb-Cre;R26-mTmG* embryos showed the expected GFP$^+$ perivascular cells (Foo et al., 2006) (Fig. 3a). In addition, we observed scattered GFP$^+$ ECs within the cardinal vein and widespread labelling of LECs within the JLS (Fig. 3a). This is consistent with recently published data showing *Pdgfrb-Cre* mediated targeting of ECs within the cardinal vein, JLS and lymphovenous valves (Turner et al., 2014), but is in contrast to findings of Klotz *et al.*, (2015) reporting absence of *Pdgfrb-Cre* mediated recombination within the E10 cardinal vein and E12.5 JLS (Klotz et al., 2015). FACS analysis of endothelial cells (Fig. 3b) further demonstrated limited but detectable *Pdgfrb-Cre* induced recombination in the blood vasculature as early as at E9 (3.5% ± 3.7% GFP$^+$ ECs, $n = 5$; Fig. 3c). The proportion of Cre-recombined ECs increased at E10 (9.3% ± 2.0%, $n = 3$), reaching a significant labelling of ECs in E12 embryos

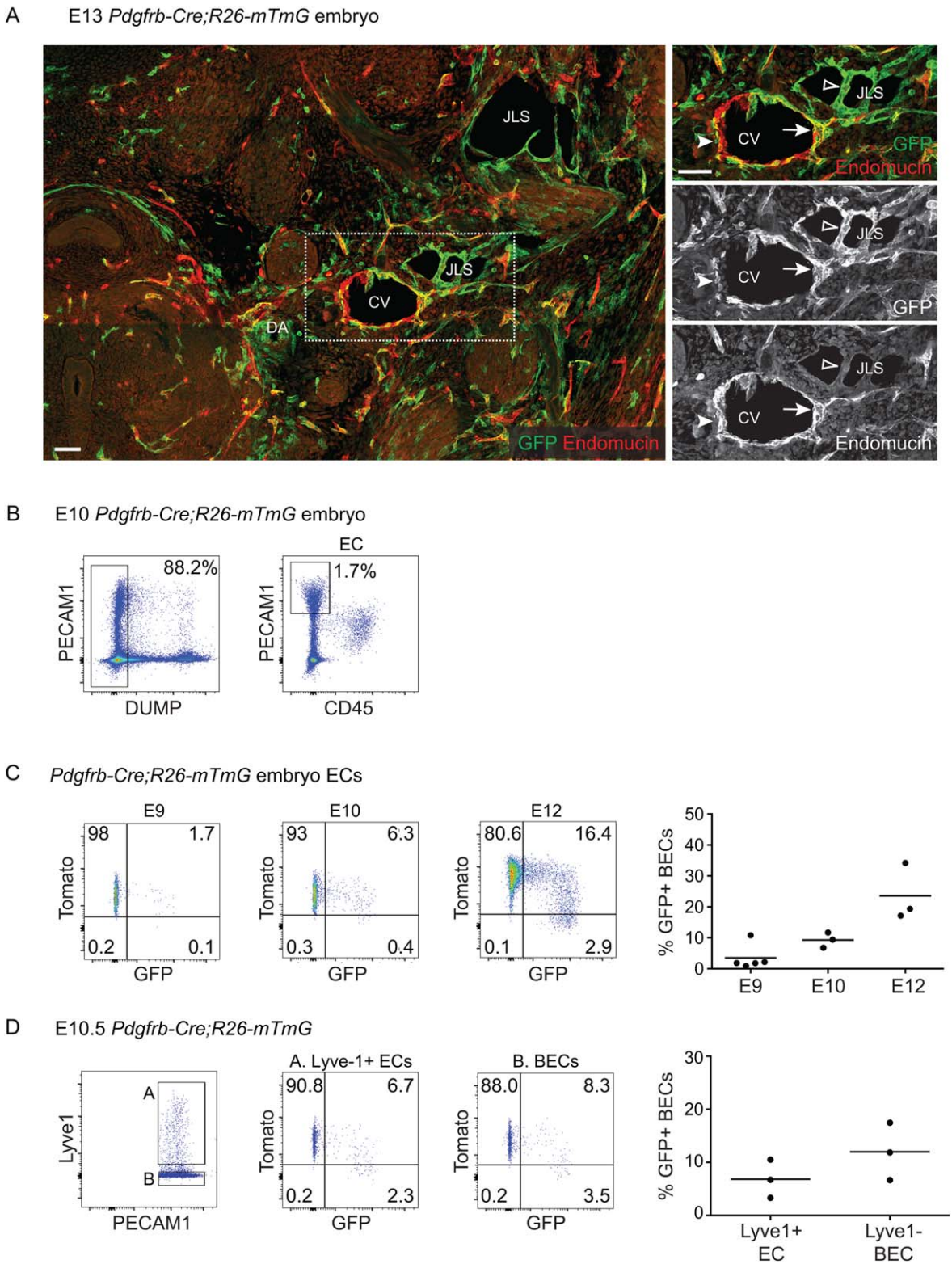

FIG. 3. *Pdgfrb-Cre* cannot differentiate between venous and non-venous derived LEC progenitors. (**A**) Immunofluorescence of a transverse vibratome section of E13.5 *Pdgfrb-Cre;R26-mTmG* embryo using antibodies against GFP (green), and Endomucin (red; marker of venous EC). Note scattered GFP-labeling of the cardinal vein (CV) and jugular lymph sac (JLS). DA = dorsal aorta. Boxed area is magnified in the small inserts to the right and single channel images are shown. Arrow points to a GFP^+ venous EC, open arrowhead to a GFP^+ LEC and arrowhead indicates a GFP^+ $Endomucin^-$ mural cell. Scale bars: 50 μm. (**B**) Gating scheme for analysis of ECs in the E10 embryo proper. After exclusion of dead cells and erythrocytes in the dump channel PECAM-1^{high} cells (ECs) are selected while $CD45^+$ $PECAM1^{intermed}$ immune cells are excluded. (**C**) Tomato and GFP expression in *Pdgfrb-Cre;R26-mTmG* embryos showing a gradual increase of GFP-labelling of the ECs between E9 and E12 ($n = 5$ (E9); $n = 3$ (E10 and E12)). (**D**) Analysis of $Lyve1^+$ (venous derived LECs and LEC progenitors) and $Lyve1^-$ ECs from E10.5 *Pdgfrb-Cre;R26-mTmG* embryos shows Cre recombination in both cell fractions. The Tomato/GFP Dot plots display 1000 event from $Lyve1^+$ and $Lyve1^-$ gates.

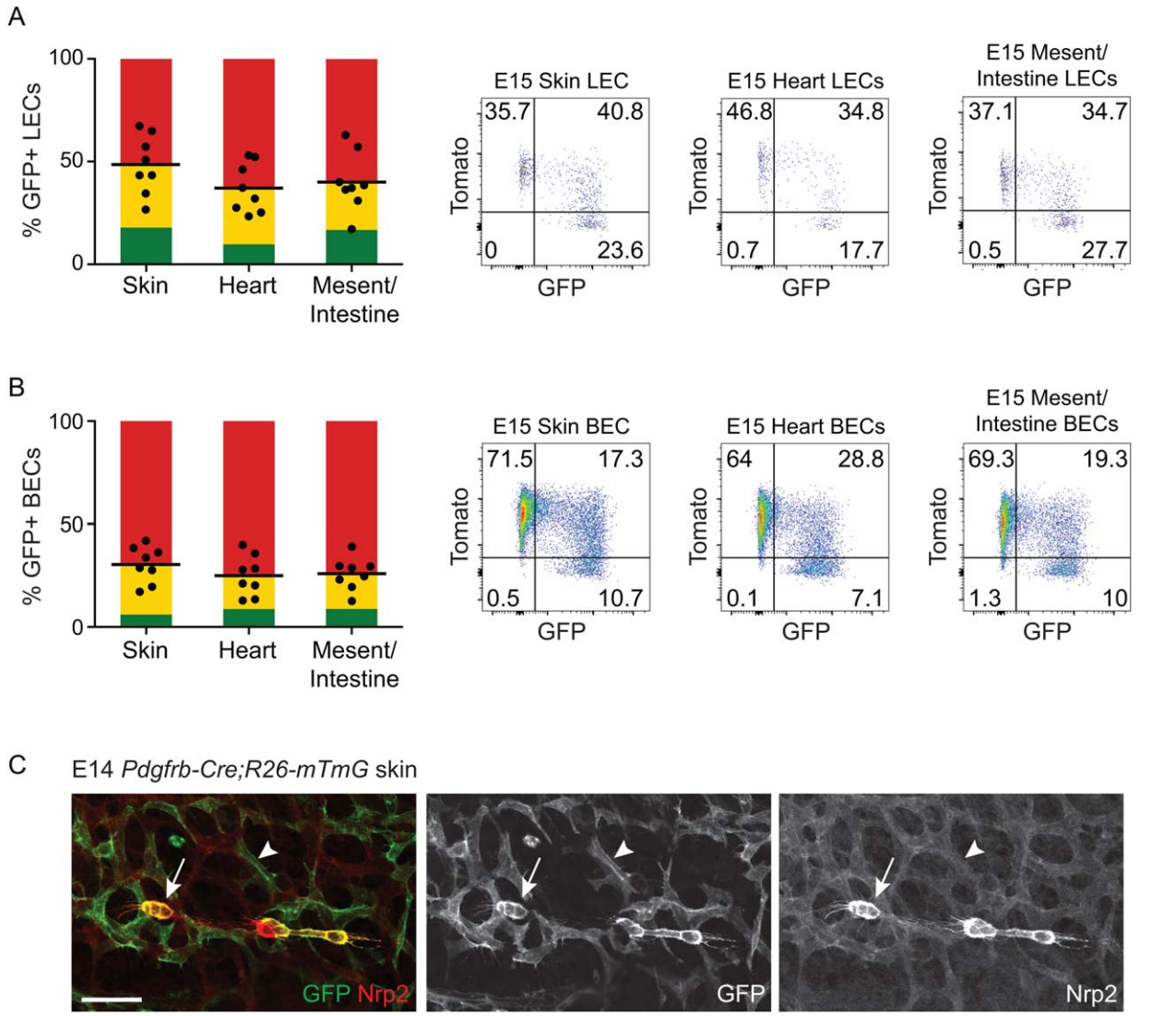

FIG. 4. *Pdgfrb-Cre* targets both BECs and LECs in multiple organs. (**A, B**) FACS analysis of LECs (**A**) and BECs (**B**) from E15 *Pdgfrb-Cre;R26-mTmG* skin, heart, and mesentery/intestine; showing a significant GFP$^+$ LEC population. Graph of all results showing the average distribution of cells expressing Tomato only (red), GFP and Tomato (yellow) and GFP only (green). Dots show % of GFP$^+$ LECs (**A**) and BECs (**B**) in individual embryos, horizontal line represents mean ($n = 8$.) On the right representative FACS plots from one embryo. (**C**) Representative single plane confocal image of E14 skin *Pdgfrb-Cre;R26-mTmG* stained with anti-Nrp2 (red) and anti-GFP (green) antibodies. Panels on the right show single channel images. Nrp2 is highly expressed in the dermal LEC clusters (arrow) while weaker expression is detected in the BECs (arrowhead). Notably, both cell types display GFP expression. Scale bar: 50 μm.

(23.5% ± 7.5%, $n = 3$; Fig. 3c). Separate analysis of Lyve1$^+$ ECs (i.e. venous derived LECs and LEC progenitors) and Lyve1$^-$ BECs in E10.5 embryos showed a similar *Pdgfrb-Cre* induced recombination in both cell fractions (Fig. 3d). In summary, these data demonstrate that *Pdgfrb-Cre* targets embryonic blood vasculature prior to initiation of venous sprouting of lymphatic vessels and shows significant labelling of ECs in the cardinal vein and the JLS. *Pdgfrb-Cre* cannot therefore be used to specifically trace and target non-venous derived LEC progenitors.

The high proportion of ECs (20–25%) targeted by the *Pdgfrb-Cre* transgene in E12 embryos and targeting of both Lyve1$^+$ and Lyve1$^-$ ECs in E10.5 embryos indicated a more widespread vascular induction than could be explained by specific *Pdgfrb-Cre* expression in the cardinal vein and developing lymph sacs. This prompted us to further analyze the blood and lymphatic vasculature of the skin, heart and the mesentery/intestine to evaluate if expression of *Pdgfrb-Cre* is specific for LECs and their progenitors. FACS analysis of E15 embryos revealed a high proportion of GFP$^+$ LECs in the skin

(48.0% ± 13.4%), the heart (36.6% ± 11.2%), and the mesentery/intestine (39.5% ± 13.4%; $n = 8$) (Fig. 4a). Surprisingly, the BECs of all analyzed organs and in all eight embryos, collected from three independent litters, also showed robust GFP expression [skin 30.1% ± 8.2%, heart 24.6% ± 9.2% and mesentery/intestine 25.5% ± 7.4%; ($n = 8$); Fig. 4b]. Immunofluorescence analysis of the skin confirmed GFP expression in dermal LECs and BECs (Fig. 4c).

Widespread Cre-labeling of ECs of multiple vascular beds raises the question of whether this reflects active or historical expression of the *Pdgfrb-Cre* transgene in ECs or their progenitors, respectively. Based on co-expression of Tomato and GFP (indicated by yellow in the stacked bars), the majority of the GFP^+ *Pdgfrb-Cre* labeled ECs in both lymphatic and blood vessels were found to be recently recombined cells (Fig. 4a,b). As a comparison, E10 YS-derived macrophages and monocytes in *Tie2-Cre*;*R26-mTmG* embryos displayed no detectable Tomato (Fig. 2c). Given that these cells originate from *Tie2-Cre* positive cells between E7 and E9, detectable Tomato was lost within 2–3 days after recombination. The high proportion of $Tomato^+GFP^+$ ECs at E15, 5 days after the loss of YS hemogenic activity, therefore suggests active expression of *Pdgfrb-Cre* in the ECs. This is unexpected since *Pdgfrb* expression has not been previously reported in ECs, and it is thought to be exclusively expressed in mural and subsets of mesenchymal cells (Andrae et al., 2008; Gaengel et al., 2009). We cannot exclude the possibility that the endothelial activity of the *Pdgfrb-Cre* line reflects recent tracing from an unknown source of *Pdgfrb* expressing EC progenitors or a transient endothelial expression of *Pdgfrb*. However, another plausible explanation is that it represents ectopic expression of the *Pdgfrb-Cre* transgene.

In conclusion, data presented here show that *Pdgfrb-Cre* does not allow selective tracing of non-venous derived LEC progenitors. *Pdgfrb-Cre* targeting of LECs also does not provide evidence for YS origin of the lymphatic vasculature. Instead, *Pdgfrb-Cre* labels a proportion of lymphatic and blood ECs in multiple organs. In light of these data, our previous conclusion that *Pdgfrb-Cre* selectively targets non-venous mesenteric LEC progenitors (Stanczuk *et al*., 2015) has to be revised. Although we have observed a specific defect in mesenteric lymphatic development in embryos with *Pdgfrb-Cre* induced deletion of the lymphatic growth factor receptor *Vegfr3* (Stanczuk *et al*., 2015), this may rather reflect the extent and timing of *Pdgfrb-Cre* activity in the mesenteric in comparison to other lymphatic vascular beds than selective targeting of the non-venous LEC progenitors. The new data does not, however, change the conclusion on the HemEC origin of the mesenteric LEC progenitors, which we based on positive lineage tracing with the hemogenic lineage marker *cKit-CreER^{T2}* and early induction of the vascular marker *Pdgfb-CreER^{T2}*, which labels all major hemogenic vessels but not venous derived LEC progenitors (Stanczuk *et al*., 2015). In the case of the heart, our data, which excludes YS origin as an explanation for *Pdgfrb-Cre* labeling of LECs, combined with the lack of endothelial cell tracing (Klotz *et al*., 2015) that would be expected for HemEC-derived progenitors, calls for further investigation into the origin of cardiac lymphatic vessels. Our data further highlight that future studies analyzing the effect of *Pdgfrb-Cre* mediated gene deletion in the mural cells must also take into account deletion in a significant portion of both blood and lymphatic ECs from early development. More generally, our results illustrate the inherent limitations of using constitutive Cre lines in lineage tracing experiments, and the careful evaluation needed to differentiate de novo expression from lineage tracing.

METHODS

Mice

Pdgfrb-Cre mice (Foo *et al*., 2006) were kindly provided by Ralf Adams (Max Planck Institute for Biomedicine, Münster, Germany). *R26-mTmG* mice (Muzumdar *et al*., 2007); obtained from the Jackson Laboratory) and *Tie2-Cre* mice (Koni *et al*., 2001) were described previously. Staging of E9 and E10 embryos were done by somite counting (sc) and Theiler stage (TS) was determined according to EMAP eMouse Atlas Project (http://www.emouseatlas.org) (Richardson *et al*., 2014). Data from E9 embryos refer to sc 15-18, TS14; E10 sc 24-26, TS15; and E10.5 sc 34-37, TS17. For embryos older than E11, the morning of vaginal plug detection was considered as E0. All strains were maintained and analyzed on C57BL/6J background.

Immunofluorescence

Yolk sac and skin were fixed in 4% paraformaldehyde (PFA) for 2 h at RT, permeabilized in 0.3% Triton-X100 in PBS (PBSTx) and blocked in PBSTx plus 3% milk. Primary antibodies were incubated at 4°C overnight in blocking buffer. After washing in PBSTx, the samples were incubated with fluorochrome-conjugated secondary antibodies in blocking PBSTx plus 3% milk, before further washing and mounting in Mowiol. For visualization of cardinal veins and lymph sacs, 150 μm vibratome cross sections of E13.5 PFA fixed *Pdgfrb-Cre;R26-mTmG* embryos were prepared and stained as described above. The following antibodies were used: chicken anti-GFP (Abcam cat 13970), rat anti-mouse Endomucin (Santa Cruz Biotechnology cat sc-65495), goat anti-mouse Neuropilin-2 (R&D Systems cat AF567), rat anti-mouse CD41 (BectonDickinson cat 553847) and goat anti-mouse VEGFR2 (R&D Systems cat AF644).

Secondary antibodies conjugated to AF488, Cy3 or AF647 were obtained from Jackson ImmunoResearch. Confocal images were acquired using Zeiss 700 confocal microscope and Zen 2009-2011 software. Figures 1G and 3A were acquired as maximum intensity projections of Z-stacks of multiple tile scan images (3 × 3 tiles), images shown in Figure 1G were cropped. Figure 4C represents a single plane. Images in Figure 1G were taken using a Plan-Apochromat 20x/0.8 Ph2 objective and Figs. 3A and 4C were taken using Plan-Apochromat 20x/0.8 M27 objective.

Flow Cytometry

E15 embryonic back skin, heart and mesentery together with intestine were harvested and digested in 4 mg ml^{-1} Collagenase IV (Life Technologies), DNase I (Roche) 0.2 mg ml^{-1} in PBS with 10% Fetal calf serum (FCS; Gibco) at 37° in a water bath for 20 min. E9 and E10 embryos were digested using a lower amount of Collagenase IV 1 mg ml^{-1} and 10% FCS, 10–15 min. E12 embryo and YS were digested in 2 mg ml^{-1} Collagenase IV, 5% FCS (Life Technologies). Digested samples were quenched by adding 2 mM EDTA and filtered through a 70 μm nylon filter (BD Biosciences). Cells were washed with FACS buffer (PBS, 0.5% FCS, 2 mM EDTA) and immediately processed for staining in 96-well plates. Fc receptor binding was blocked by rat anti-mouse CD16/CD32 (93) (eBioscience). E15 samples were stained with anti-CD31/PECAM-1 (390) PE-Cy7, anti-podoplanin (PDPN) eF660 (eBio8.1.1) (both from eBioscience). Dump channel included markers to exclude immune cells anti-CD45 (30-F11); macrophages, anti-F4/80 (BM8), myeoloid cells, anti-CD11b (M1/70) and red blood cells, anti-TER-119 (TER-119); all conjugated with eF450 (eBioscience); together with Sytox blue (Life Technologies) for dead cell exclusion. E15 LECs and BECs were gated in two steps; 1. $PECAM1^{high}$, dump $channel^{negative}$ cells. 2. $PDPN^{positive}$ (LECs) $PDPN^{negative}$ (BECs). E9 and E10 YS and embryos were stained with anti-CD31/PECAM-1 (390) PE-Cy7, anti-c-Kit/CD117 (2B8) APC, anti-CD11b (M1/70) Percp-Cy5.5, anti-CD45 (30-F11) APC-eF780. Anti-TER-119 (TER-119) e450 and Sytox blue (Invitrogen; to detect dead cells) were included in the dump channel. For E12 embryos anti-CD11b (M1/70) and anti-F4/80 (BM8) were included in the dump channel as described for E15 samples. The anti-rat/hamster compensation bead kit (Life Technologies) was used for compensation controls, with the addition of Tomato positive tissue and GFP positive tissue for Tomato and GFP compensation. The cells were analyzed on a FACSariaIII cell sorter with the FACSDiva software (all from BD biosciences). Data were processed using FlowJo software (TreeStar). Single cells were gated using FSC-A/SSC-A followed by FSC-H/FSC-W and SSC-H/SSC-W in all experiments.

ACKNOWLEDGMENT

The author thanks Ralf Adams (Max Planck Institute for Molecular Biomedicine, Münster) for providing the *Pdgfrb-Cre* mice and BioVis at Uppsala University for help with flow cytometry experiments.

LITERATURE CITED

Abraham S, Kogata N, Fassler R, Adams RH. 2008. Integrin beta1 subunit controls mural cell adhesion, spreading, and blood vessel wall stability. Circ Res 102:562–570.

Andrae J, Gallini R, Betsholtz C. 2008. Role of platelet-derived growth factors in physiology and medicine. Genes Dev 22:1276–1312.

Antas VI, Al-Drees MA, Prudence AJ, Sugiyama D, Fraser ST. 2013. Hemogenic endothelium: A vessel for blood production. Int J Biochem Cell Biol 45:692–695.

Foo SS, Turner CJ, Adams S, Compagni A, Aubyn D, Kogata N, Lindblom P, Shani M, Zicha D, Adams RH. 2006. Ephrin-B2 controls cell motility and adhesion during blood-vessel-wall assembly. Cell 124:161–173.

Gaengel K, Genove G, Armulik A, Betsholtz C. 2009. Endothelial-mural cell signaling in vascular development and angiogenesis. Arterioscler Thromb Vasc Biol 29:630–638.

Gomez Perdiguero E, Klapproth K, Schulz C, Busch K, Azzoni E, Crozet L, Garner H, Trouillet C, de Bruijn MF, Geissmann F, Rodewald HR. 2015. Tissue-resident macrophages originate from yolk-sac-derived erythro-myeloid progenitors. Nature 518:547–551.

Greif DM, Kumar M, Lighthouse JK, Hum J, An A, Ding L, Red-Horse K, Espinoza FH, Olson L, Offermanns S, Krasnow MA. 2012. Radial construction of an arterial wall. Dev Cell 23:482–493.

Hagerling R, Pollmann C, Andreas M, Schmidt C, Nurmi H, Adams RH, Alitalo K, Andresen V, Schulte-Merker S, Kiefer F. 2013. A novel multistep mechanism for initial lymphangiogenesis in mouse embryos based on ultramicroscopy. Embo J 32:629–644.

Henderson NC, Arnold TD, Katamura Y, Giacomini MM, Rodriguez JD, McCarty JH, Pellicoro A, Raschperger E, Betsholtz C, Ruminski PG, Griggs DW, Prinsen MJ, Maher JJ, Iredale JP, Lacy-Hulbert A, Adams RH, Sheppard D. 2013. Targeting of alphav integrin identifies a core molecular pathway that regulates fibrosis in several organs. Nat Med 19:1617–1624.

Hoeffel G, Chen J, Lavin Y, Low D, Almeida FF, See P, Beaudin AE, Lum J, Low I Forsberg EC, Poidinger M, Zolezzi F, Larbi A, Ng LG, Chan JK, Greter M, Becher B, Samokhvalov IM, Merad M, Ginhoux F. 2015. C-Myb(+) erythro-myeloid progenitor-derived fetal monocytes give rise to adult tissue-resident macrophages. Immunity 42:665–678.

Jeansson M, Gawlik A, Anderson G, Li C, Kerjaschki D, Henkelman M, Quaggin SE. 2011. Angiopoietin-1 is essential in mouse vasculature during development and in response to injury. J Clin Investig 121:2278–2289.

Klotz L, Norman S, Vieira JM, Masters M, Rohling M, Dube KN, Bollini S, Matsuzaki F, Carr CA, Riley PR. 2015. Cardiac lymphatics are heterogeneous in origin and respond to injury. Nature 522:62–67.

Kogata N, Tribe RM, Fassler R, Way M, Adams RH. 2009. Integrin-linked kinase controls vascular wall formation by negatively regulating Rho/ROCK-mediated vascular smooth muscle cell contraction. Genes Dev 23:2278–2283.

Koni PA, Joshi SK, Temann UA, Olson D, Burkly L, Flavell RA. 2001. Conditional vascular cell adhesion molecule 1 deletion in mice: Impaired lymphocyte migration to bone marrow. J Exp Med 193:741–754.

Martinez-Corral I, Ulvmar M, Stanczuk L, Tatin F, Kizhatil K, John SW, Alitalo K, Ortega S, Makinen T. 2015. Non-venous origin of dermal lymphatic vasculature. Circ Res.

Medvinsky A, Rybtsov S, Taoudi S. 2011. Embryonic origin of the adult hematopoietic system: Advances and questions. Development 138:1017–1031.

Muzumdar MD, Tasic B, Miyamichi K, Li L, Luo L. 2007. A global double-fluorescent Cre reporter mouse. Genesis 45:593–605.

Richardson L, Venkataraman S, Stevenson P, Yang Y, Moss J, Graham L, Burton N, Hill B, Rao J, Baldock RA, Armit C. 2014. EMAGE mouse embryo spatial gene expression database: 2014 update. Nucleic Acids Res 42:D835–D844.

Siegenthaler JA, Choe Y, Patterson KP, Hsieh I, Li D, Jaminet SC, Daneman R, Kume T, Huang EJ, Pleasure SJ. 2013. Foxc1 is required by pericytes during fetal brain angiogenesis. Biol Open 2:647–659.

Srinivasan RS, Dillard ME, Lagutin OV, Lin FJ, Tsai S, Tsai MJ, Samokhvalov IM, Oliver G. 2007. Lineage tracing demonstrates the venous origin of the mammalian lymphatic vasculature. Genes Dev 21:2422–2432.

Stanczuk L, Martinez-Corral I, Ulvmar MH, Zhang Y, Lavina B, Fruttiger M, Adams RH, Saur D, Betsholtz C, Ortega S, Alitalo K, Graupera M, Makinen T. 2015. cKit lineage hemogenic endothelium-derived cells contribute to mesenteric lymphatic vessels. Cell Rep 10:1708–1721.

Stenzel D, Nye E, Nisancioglu M, Adams RH, Yamaguchi Y, Gerhardt H. 2009. Peripheral mural cell recruitment requires cell-autonomous heparan sulfate. Blood 114:915–924.

Turner CJ, Badu-Nkansah K, Crowley D, van der Flier A, Hynes RO. 2014. Integrin-alpha5beta1 is not required for mural cell functions during development of blood vessels but is required for lymphatic-blood vessel separation and lymphovenous valve formation. Dev Biol 392:381–392.

Yang Y, Garcia-Verdugo JM, Soriano-Navarro M, Srinivasan RS, Scallan JP, Singh MK, Epstein JA, Oliver G. 2012. Lymphatic endothelial progenitors bud from the cardinal vein and intersomitic vessels in mammalian embryos. Blood 120:2340–2348.

Ye X, Wang Y, Cahill H, Yu M, Badea TC, Smallwood PM, Peachey NS, Nathans J. 2009. Norrin, frizzled-4, and Lrp5 signaling in endothelial cells controls a genetic program for retinal vascularization. Cell 139:285–298.

You WK, Yotsumoto F, Sakimura K, Adams RH, Stallcup WB. 2014. NG2 proteoglycan promotes tumor vascularization via integrin-dependent effects on pericyte function. Angiogenesis 17:61–76.